A Novel Multiple Linear Multivariate NIR Calibration Model-Based Strategy for In-Line Monitoring of Continuous Mixing

Leonel Quiñones and Carlos Velazquez
Dept. of Chemical Engineering, University of Puerto Rico at Mayaguez, Mayaguez, PR 00681

Luis Obregon
Dept. of Chemical Engineering, Universidad del Atlántico, Barranquilla, Colombia

DOI 10.1002/aic.14498
Published online June 2, 2014 in Wiley Online Library (wileyonlinelibrary.com)

The capability of near infra-red (NIR) spectroscopy to predict many different variables, such as concentration and humidity, has been demonstrated in many published works. Several of those articles have been in the subject of real time prediction of continuous operations. However, those demonstrations have been for narrow ranges of the variables, especially for powder concentration, which could present a nonlinear behavior of the NIR absorbance as a function of the entire range of concentration. This work developed a novel strategy to predict the entire range of powder concentration using multiple linear NIR calibration models. The root mean standard error of prediction and relative standard deviation (RSD) parameters were used to establish the number of the multiple linear calibration models; other statistical features were used to establish the correct prediction. It was found that a minimum number of linear partial least squares (PLS) calibration models were necessary to accurately predict the range from 0 to 100% w/w. This technique could also be used with other nonlinear behaviors. © 2014 American Institute of Chemical Engineers *AIChE J*, 60: 3123–3132, 2014
Keywords: near-infrared spectroscopy, linear partial least squares calibration models, nonlinear calibration curves, Process Analytical Technologies, in-line near infra-red monitoring, continuous mixing

Introduction

Many studies have demonstrated that due to near infra-red (NIR) spectroscopy's nature, it has the capability to measure: powder humidity,[1–4] particles size,[3,5–8] powder mixture homogeneity and segregation,[9–20] particle and tablet coating,[21] chemical and biochemical reactions,[22–24] adsorption and desorption phenomena,[25–27] crystal synthesis and crystal growth[5,27] among others. These very same publications have developed the methodology to construct the calibration models, which are based mainly on linear correlations.

NIR spectroscopy is a nondestructive analytical method that acquires highly valuable physical and chemical information with little or no sample preparation that can be used to monitor powder processing. The advance in NIR spectrophotometers, specifically in the high-speed data transmission, and the use of multivariate software, has increased the possibility to implement this sensor in-line for continuous powder processing.[10,15,16,28]

Changes in active pharmaceutical ingredient (API) concentration are specifically reflected in certain wavelength ranges after a spectral pretreatment, such as standard normal variate (SNV) and first or second derivative transformation. The pretreatment insures the construction of more robust mathematical calibration models, using, for example, partial least squares (PLS) to predict not only the API concentration of pharmaceutical blends,[10] but possibly other components. This capacity helps monitor not only powder mixing, but also other powder processes, allowing to test in-line the quality of production with no need of sample preparation.

Despite the capacity to monitor different processing units, a comprehensive study of the monitoring of a pharmaceutical continuous line has not been performed. Such a study, to further automate all of the steps of a continuous line, will require the characterization of the continuous mixing process as a first step. This characterization could be based on a solid mathematical model constructed from NIR spectra, taken in-line from the mixer.[10,15,16,28] However, due to the fact that in continuous processing, there is always the possibility of process perturbations caused by external factors, such as an increase or decrease in the electric power, refilling, and so forth, large changes in drug formulation may occur, making necessary the existence of a robust mathematical model able to predict in the full range of concentration. Shao et al.[29] concluded that it is not possible to achieve an adequate exactitude in the predictions using just one model for a wider or the entire range.[30] The main reason is the nonlinear behavior that exhibits the radiation absorbance as a function of the solute concentration and deviation from the linear Beer's law.

Balabin et al.[30] specifically compared linear vs. nonlinear (Poly-PLS, Spline-PLS, and Neural Network) models to

Correspondence concerning this article should be addressed to C. Velazquez at carlos.velazquez9@upr.edu.

Table 1. Powders' Properties Description

Powders	Naproxen Sodium	Monohydrate Lactose Tablettose 70 (NF, EP, JP)	Magnesium Stearate (NF)
Manufacturer	BASF Corporation	Mutchler Inc.	Mallinckrodt Inc.
Bulk density (g/cm^3)	0.93	0.592	0.37
Cohesion (Kpa)	0.98	0.01	0.38
Carr index	44.4	14.7	34.2
Mean particle size (mm)	29	168	6
Standard deviation (mm)	20	90	3.5

predict gasoline properties based on NIR data. The main conclusion was that the nonlinear models made the best prediction. A characteristic of nonlinear models is that the structure of the model (number of dots and degree [2 degree of freedom] in Spline-PLS, degree and nonlinear terms [2 degree of freedom] in Poly-PLS, and number of neurons [1 degree of freedom] in artificial neural network (ANN)) must be fixed beforehand, which could limit the precision. A solution could be to build on the Spline-PLS approach by breaking the curve of the entire range in multiple linear segments [1 degree of freedom], as it will be explained later in Results section. Each smaller linear segment would then be represented by a linear multivariate PLS calibration model developed for that smaller range, which will produce a higher accuracy of the linear multivariate calibration model for that specific range. In this way, the simplicity of the structure of the linear model and the approximation of the nonlinear curve by multiple linear segments are combined for a better prediction.

The issue, though, is how to select the right mathematical model to predict the in-line concentration based on the actual NIR spectrum. As NIR absorbance is highly sensitive to many factors, especially those involved during continuous operation, there is a real possibility of choosing the wrong model. To select the right model, it is necessary to use statistical features that look at the raw NIR spectrum and are able to discriminate, among all the models, which one was developed with similar spectrum pattern.

Therefore, this study focused on the development of this approach to approximate the nonlinear curve of the entire range, from 0 to 100% w/w of the target component, with a number of smaller linear segments; these will cover the entire range and each smaller linear segment will be fitted with a robust linear multivariate NIR calibration models developed using the PLS technique. All the models together will predict the entire range with more accuracy than just one linear model for the entire nonlinear range.[30] The models were created using in-line NIR data, taking into account all the variability of the system, and the standard procedure suggested in the literature. Two statistical parameters ($D_{\text{mod}}X$ and T^2) were used to select, among the models making the predictions, the model that produced the correct prediction. $D_{\text{mod}}X$ is the minimum distance of an observation to the model (see Appendix for more details), and the Hotelling T^2 statistics is a combination of all the $\boldsymbol{t}$ scores in a selected range of components.[31]

The next section describes the materials and equipment used for the experimentation, and the procedures to collect and analyze the NIR data. The section of results demonstrates the nonlinear behavior of the absorbance, the novel approach to approximate the nonlinear curve with multiple linear PLS multivariate calibration models, the accuracy of the multiple linear models, how to select the minimum number of linear models necessary to approximate the entire range, and how to select the correct prediction using the aforementioned statistics. It was demonstrated that these models and the statistical parameters accurately predicted the actual concentration in real time. A future use of this novel approach is the in-line monitoring, control, and optimization of continuous processes.

Experimental Work

Materials

The materials used included: Naproxen Sodium (used as the API), lactose monohydrate (Tablettose 70), and magnesium stearate (MgSt) as excipients. The powders were characterized using a powder rheometer (FT4—Freeman Technologies) and a particle-size analyzer (Insitec-Malvern). Table 1 shows the materials used with their respective physical properties.

Equipment

Feeder and Calibration. The mixtures of Naproxen, lactose, and MgSt were placed in the Gericke powder feeder (Figure 1), which was always filled at the beginning of each run up to approximately 80% of its maximum capacity (0.032 m^3) and operated at constant screw speed. For the calibration, the feeder screw speed was set at different percentages of the maximum speed to obtain different powder flow rates. Material was collected at the exit of the feeder every 5 s, and then weighed to calculate the flow rate. This procedure was repeated for several setting percentages (between 0 and 100%) to complete the flow rate calibration curve.

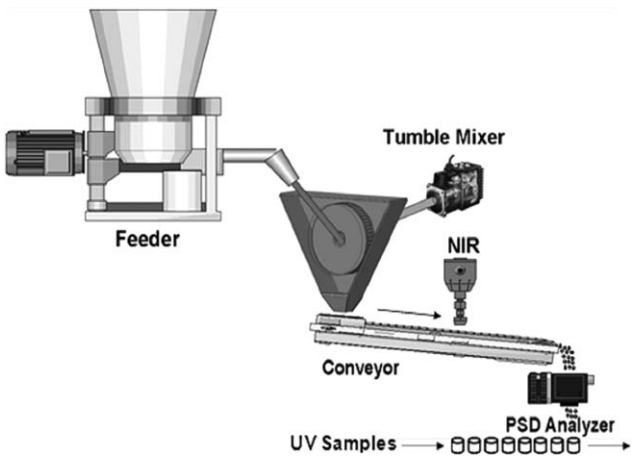

Figure 1. Schematic of the experimental system.

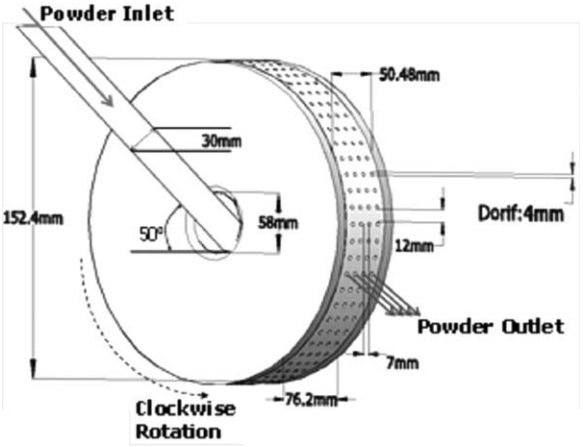

Figure 2. Schematic of the continuous tumble mixer.

Continuous Mixing Unit. The continuous mixing equipment used for the experiments was a low shear tumble mixer (Figures 1 and 2 for more details), which consisted of a cylinder made of acrylic to allow visual inspection of the internal powder mixing behavior. The cylinder is connected from one of its ends to the shaft of a variable speed motor, which permits control of the rotation at different rpm. The other end has a hole in the center that permits the entrance of the powders from an acrylic tube of 25.4 mm of internal diameter and an inclination of 50° with respect to the horizontal, to facilitate the powder flowability toward the tumble. The cylinder has 152.4 mm of internal diameter with multiple orifices; each of 4 mm in diameter and 6.35 mm in depth, see Figure 2. The mixer rotates making the powder particles form an avalanche while they leave the mixer at the same time through the orifices by the effect of centrifuge forces.

Conveyor Belt. A conveyor belt was placed below the exit of the tumble mixer to catch the powders and move them to the next process. The width of the belt was about 0.56 m (bigger than the diameter of the NIR spot, 0.025 m), and its speed was set at a linear velocity of 0.16 m/s to insure a height of the powder bed above the belt at approximately 0.005 m in average, for the powder flow rate used through the continuous mixer. The conveyor belt was used to help present the powders to the NIR in a consistent manner to acquire spectral data of the sample with constant conditions. This is essential to ensure accuracy and precision of the NIR sensor.

V-Blender. This blender was used to prepare the powder blends, with concentration of the Naproxen ranging from 0 to 100% w/w, that were later sensed in-line with the NIR. The mixer is asymmetric with a volume capacity of approximately 0.027 m^3, made up by two hollow cylindrical stainless steel shells of 0.229 m in diameter and different heights (0.533 and 0.457 m) joined at an angle of 70°.

Instrumentation

NIR. A self-referencing NIR spectrophotometer from Control Development (CDI), series SNIR 1402, was used to acquire the in-line spectra of the powders being transported by the conveyor belt. The spectrophotometer has InGaAs detectors providing a spectral range from 900 to 1700 nm at a resolution of 1 nm. The diffuse reflectance measurement probe has an illumination spot with a diameter of 0.025 m and with a depth in radiation penetration of about 0.4 mm. The penetration depth was determined experimentally, varying the height of the powder over a piece of material capable of absorbing NIR radiation. The minimum height of powder that allowed the radiation to reach the piece of material and as such to alter the NIR spectrum was fixed as the penetration depth. This spectrophotometer communicated to the computer via USB2.0 interface through which the spectra were transmitted using the data acquisition package CDI Spec32^{TM} version 1.7.1.3. The spectra (an average of 20 spectra) were taken in dynamic mode with an integration time of 0.0066 s. The data were analyzed using the software SIMCA P+, UMETRICS.

The process to develop the NIR linear multivariate PLS calibration models included: (1) the pretreatment of the NIR spectra with the SNV technique, (2) computation of the first derivative using the Savitzky–Golay algorithm with seven points, and (3) finally, the application of the PLS technique to the treated data. The linear multivariate calibration models were created applying crossvalidation technique leaving 15% of the total data calibration set for validation to calculate the root mean square errors of cross validation (RMSECV). An additional set of experiments was performed and the data collected were used to calculate the root mean standard error of prediction (RMSEP).

The range of spectra used was taken considering a diagram called variable importance plot (VIP), which summarizes the overall contribution of each *X*-variable to the PLS model. The mass of the sample size (112 mg) was calculated considering the diameter of the NIR spot, the depth in penetration, the scanning integration time, the velocity of the conveyor, and the bulk density of the powder.

Off-line Ultraviolet. The mixing homogeneity of the powder blends to be in-line sensed by the NIR was double-checked using off-line ultraviolet (UV) spectroscopy (Thermo Scientific, GENESYS 10S UV VIS spectrophotometer), which required also a calibration curve. The Naproxen absorbance was read at a wavelength of 318 nm. Samples were prepared for the calibration curve, as well as new solutions to validate the UV calibration model. The quality of the UV calibration curve was confirmed by computing the RMSECV and the RMSEP, which were 0.091 and 0.07, respectively.

Experimental procedure to collect NIR data

A preblend of lactose monohydrate and 1% w/w MgSt was prepared in the V-blender. Three layers of lactose and two layers of MgSt were placed alternated inside the blender. The powders were blended at 15 RPM for 3 min to avoid overlubrication of the powder. The mixture was then withdrawn from the blender and placed in alternate layers with the Naproxen corresponding to the percentage required. Five layers of powders in total were placed inside the V-blender again and mixed at 15 RPM for 5 min. Forty-four calibration blends, ranging in drug concentration from 0 to 100% (w/w), were prepared in the same way, varying at increments of about 1% (w/w) from 0 to 30% and from 30 to 100% (w/w) at increments of about 5% (w/w). The required homogeneity in all the prepared blends was confirmed with the UV spectrophotometer and NIR absorbance data taken of the static samples.

More samples were prepared in the range from 0 to 30% to have a better description of the region where the properties of the blend are governed by the lactose. For the range 30–100%, the blend was sampled less, as the API dominates

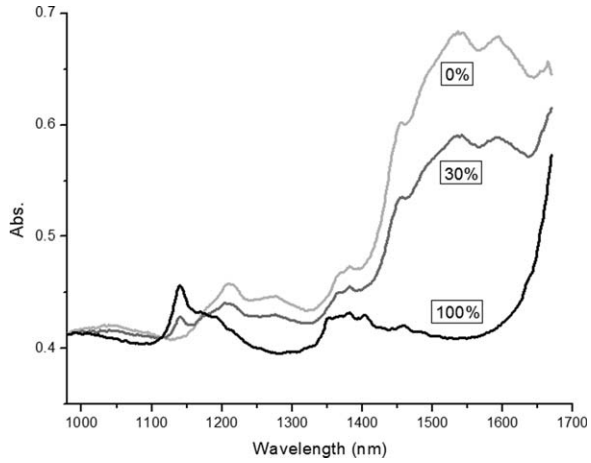

Figure 3. NIR spectra for Naproxen blends with 0, 30, and 100% (w/w).

this region, which caused a more linear behavior. However, this sampling rate can be adjusted to the needs of the user considering the behavior of the materials. The key issue is to sample at the largest interval without decreasing the accuracy of the models, but to reduce the waste of materials.

The NIR calibration models were made using the data collected dynamically to take into consideration the operating conditions of the system that could affect the particle distribution and the concentration as well. The feeder was filled up to 80% of its maximum capacity with the prepared Naproxen mixtures chosen randomly. Then, the mixture was fed to the continuous tumble mixer by the Gericke feeder at a rate of 64 kg/h. As the powders exited the tumble mixer, they fell over the conveyor belt, which moved them at a linear velocity of 0.16 m/s. The conveyor was used to help maintain a constant bulk density, which decreased the possibility of any effect of porosity changes in the NIR spectra. The NIR device, collecting continuously the spectra, was located at a distance of 5 mm from the surface of the powers. The procedure was repeated with the next random mixture until completing the 44 blends.

Results and Discussion

Nonlinear behavior

The first step was the collection of the NIR spectra, as discussed above, for the development of the linear calibration models to predict the concentration of the target component or API. Figure 3 depicts the NIR spectra for 0, 30, and 100% API (w/w). The larger spectral changes with respect to API concentration were shown in the wavelengths from 980 to 1670 nm, being the greatest intensity due to the concentration of Naproxen at 1140 nm. Conversely, the greatest intensity of the excipient was reflected in the spectrum band at 1550 nm.

Two key features are depicted in Figure 3, confirming the nonlinear relationship between the change in absorbance and the change in concentration for a wide range of concentration.[10] The first is the change in the profile of the absorbance for the selected range as the API concentration increased, and the second is that the rate of change in absorbance at 1550 nm from 0 to 30% (0.316 Abs/% conc.) is different than the one from 30 to 100% (0.25 Abs/% conc.). This change in slope confirms the nonlinearity of the entire range.

A principal component analysis (PCA) calculated for the entire calibration set data (Abs vs. 0–100% API) is shown in Figure 4, which shows the score plots of Principal Component 1 (PC1) vs. Principal Component 2 (PC2). As can be seen, there are several clusters outside of the 99% confidence limit, represented by the circle, demonstrating that one linear model for the entire range could not be sufficient to describe

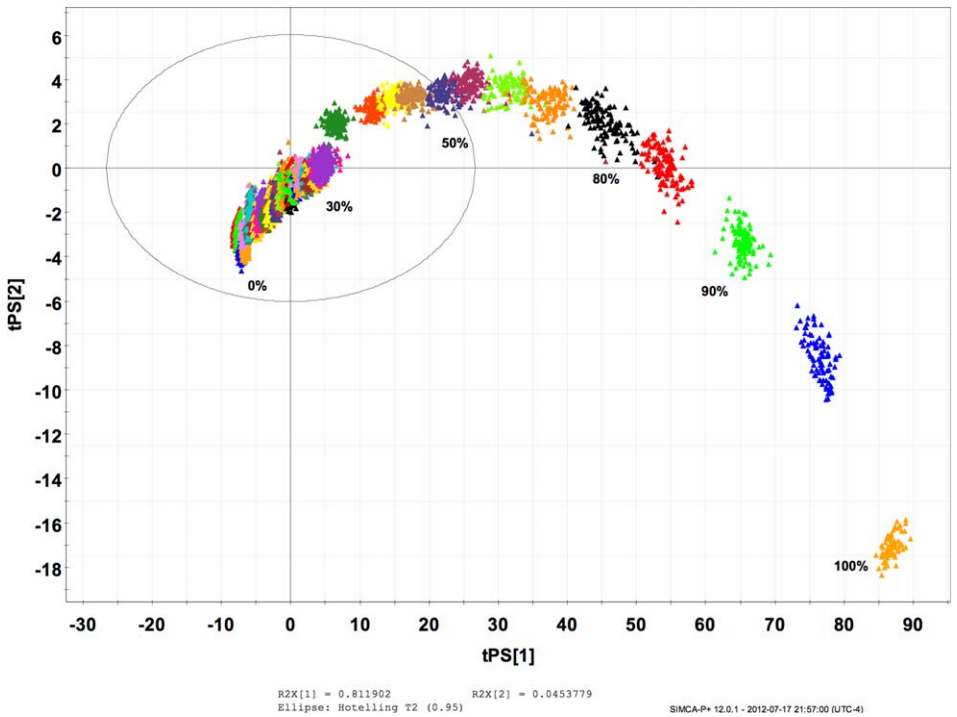

Figure 4. Scores plot from PCA of the calibration set spectra: spectrum range selected using the SIMCA P + VIP function.

[Color figure can be viewed in the online issue, which is available at wileyonlinelibrary.com.]

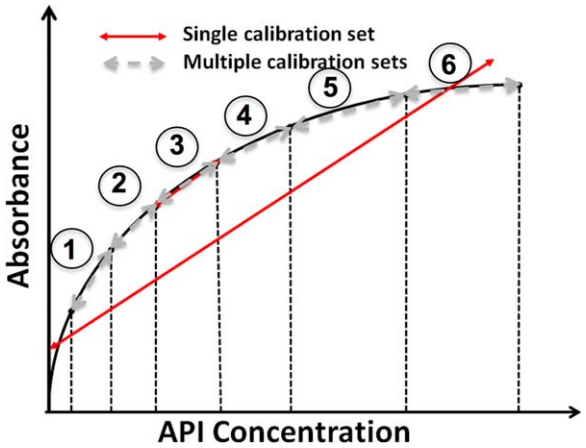

Figure 5. Approximation of the nonlinear behavior of absorbance vs. API concentration by a single linear model and six multiple linear models.

[Color figure can be viewed in the online issue, which is available at wileyonlinelibrary.com.]

the behavior of the entire range. Moreover, the clusters for an API concentration range from 0 to 50% were located inside the circle and can be represented by a straight line. Conversely, the clusters of the concentration range from 50 to 100% were located outside the PCA confident limit and with a rate of change of the PCs vs. concentration that is not linear and different than the one from 0 to 50%.

For the 0 to 50% API blends, the excipients dominate, especially toward the diluted blends, the mechanical properties, and the NIR absorbance. For the 50–100% API, the API dominates the mechanical properties and NIR absorbance, which are different than the ones for the 0–50% range as they are chemically different. Therefore, a single linear calibration model for the entire range of API concentrations will produce inaccurate predictions in some regions.

To reduce the inaccuracies due to the nonlinearity, a novel approach based on multiple linear multivariate PLS calibration models was developed to describe the nonlinear behavior of the absorbance curve for the entire range. The idea was to divide the large concentration range of the API into smaller linear segments, as shown in Figure 5, and then an independent linear multivariate PLS calibration model was adjusted for each segment,[29] using only spectral data of that segment. In theory, an infinite number of linear smaller segments will perfectly match a larger nonlinear curve. However, a finite number of linear segments should be used in practice. Again, each linear multivariate PLS calibration model was developed following the already proven methodology published in the literature.

The sets of multiple linear multivariate PLS calibration models studied are described in Table 2. The letter A corresponds to the number of models (segments) in each calibration set. For example, when A is equal to 2, the model set has two different multiple linear multivariate PLS calibration models, one covering the range from 0 to 50% API, and the other covering from 50 to 100%. In this work, several number of segments were tried to show its impact on the capacity to describe a nonlinear behavior. In practice, the number of segments to be developed should be based on the size of the entire range and the curvature of the relationship between Abs vs. concentration. This number could be established *a priori* by plotting concentration vs. absorbance, and then drawing linear segments along the entire curve, very similar to Figure 5, until the curvature is overlapped or approximated by the linear segments. This theoretical number of segments (say n) will establish the different concentration ranges that will be predicted by a linear model and will be the number of linear multivariate PLS calibration models that must be developed. To determine the best description, $(n - 1)$ and $(n + 1)$ models could be tested to verify which set of linear multivariate PLS calibration models better predict the entire range. This approach decreases to minimum the material and time required to develop the best possible set of linear multivariate PLS calibration models.

Development of the multiple linear multivariate calibration models using PLS

The NIR spectral data generated for all the 44 different API concentrations were used to develop the linear multivariate PLS calibration models; for MCS-1 (one model), the whole set was used at once; whereas from MCS-2 through MCS-9, the complete spectral set was divided accordingly to the number of models and its respective range of concentration.

The prediction precision of each set was determined using validation blends with API concentrations different than the one used in the development. The accuracy of the multiple calibrations set was evaluated using the statistical mathematical features: RMSEP and relative standard deviation (RSD).

Three concentrations were selected to demonstrate the benefits of using multiple calibration sets. The concentrations of the mixtures were: 2% (relatively low), 20% (intermediate), and 95% API (high). These values were different than the concentrations used for the calibration model and selected to assess the impact on the prediction of big changes in concentrations that could occur at the outlet of the continuous mixer in a manufacturing process.

The RMSEP results of the 2% API validation blend vs. MCS-A are depicted in Figure 6a. The RMSEP had a tendency to decrease as the number of segments (A) of the

Table 2. Concentration Range of Each PLS Model in the Multiple Calibration Sets-A (MCS-A)

MCS-A								
MCS-1	MCS-2	MCS-3	MCS-4	MCS-5	MCS-6	MCS-7	MCS-8	MCS-9
0–100%	0–50% 50–100%	0–30% 30–50% 50–100%	0–30% 30–50% 50–75% 75–100%	0–15% 15–30% 30–50% 50–75% 75–100%	0–10% 10–15% 15–30% 30–50% 50–75% 75–100%	0–5% 5–10% 10–15% 15–30% 30–50% 50–75% 75–100%	0–5% 5–10% 10–15% 15–20% 20–30% 30–50% 50–75% 75–100%	0–5% 5–10% 10–15% 15–20% 20–25% 25–30% 30–50% 50–75% 75–100%

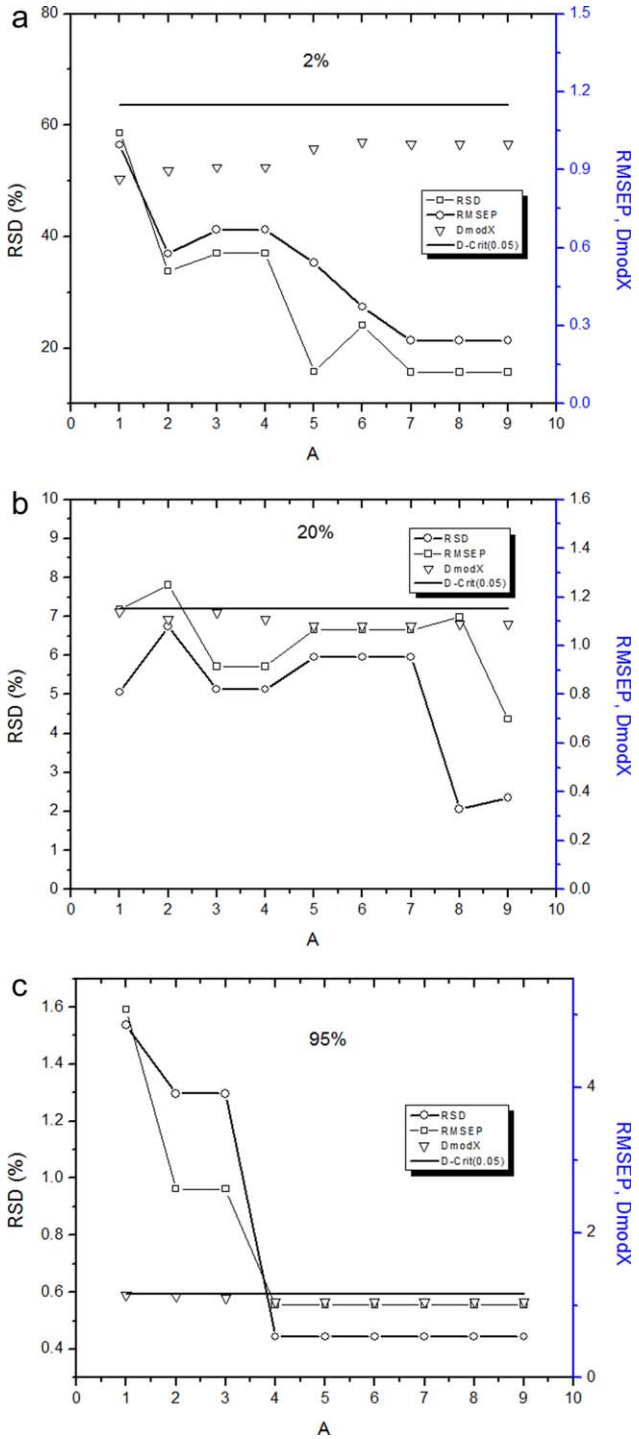

Figure 6. Accuracy of in-line NIR prediction of the validation blends [(a) 2%, (b) 20%, and (c) 95% of API] as a function of the number of linear model (MCS-A) in the calibration set.

[Color figure can be viewed in the online issue, which is available at wileyonlinelibrary.com.]

multiple linear model calibration set increased up to a certain number of models beyond, which the RMSEP kept constant at the minimum possible value. Similar result was obtained for the 95% blend as depicted in Figure 6c. Figure 6b had a slightly different behavior where the RMSEP kept almost constant at the beginning to then decrease after nine models. This is an interesting case where the user could decide to use just three or four models as the RMSEP obtained is close to the one obtained with nine models. This is an advantage of the approach that allows the user to select the number of models that best fit the monitoring objectives.

Another statistical parameter that decreased considerably as the number of calibration set increased was the RSD. As can be seen from all Figure 6, the calibration set with six models or more produced for the three concentrations the best prediction, being the lower RSD value achieved with a multiple linear multivariate PLS model calibration set of nine models. Therefore, the curve of NIR absorbance vs. concentration for the formulation studied in this work can be accurately approximated by a minimum of six linear multivariate NPLS calibration models. Figure 6a depicts an interesting result where it can be seen that the RSD is bigger than 10%. In practice, this is a too high value, which would not be accepted by the Food and Drug Administration (FDA) as a well-mixed blend; see Figure 11 for the FDA criterion. Figure 6a is for the diluted blend (2% of API), which poses several challenges to achieve an adequate degree of mixing. Considering that the approach met the FDA acceptable criterion for RSD for the other concentrations and knowing that low API concentrations have been challenging for NIR prediction, the high RSD in Figure 6a is most likely a result of the operating conditions rather than a failure of the approach.

Conversely, the prediction using a set of nine models produced a lower RMSEP for the 2% API concentration than for the concentrations of 20 and 95%. These results were related to the properties of the mixture rather than the NIR technique; the cohesiveness of the blends (Table 1) increased significantly at high concentrations of Naproxen and, therefore, the mixing and flow pattern were different. The high cohesiveness resulted in poor flow of the material and, therefore, the ingredients were poorly distributed in the mixture. This caused the prediction to have a great variability and a large error at high concentrations.

The figures also include the parameter $D_{\mathrm{mod}}X$, represented by the symbol ∇, with values for the validation samples below the critical $D_{\mathrm{mod}}X$ (D_{crit}). This means that the spectral data of the validation blends were similar to the spectral data used to build the calibration model and, therefore, that model was suitable to perform its prediction. For more details of the parameter $D_{\mathrm{mod}}X$, see Appendix.

Strategy to select the correct predicting model

The key requirement in the implementation of the idea of using multiple linear multivariate PLS calibration model sets, such as MCS-9, for the in-line monitoring would be the selection of the adequate model to perform the prediction in real time. As the concentration is not known *a priori*, all the models must be enabled to perform predictive calculations and, then, the correct concentration can be selected. A strategy to choose the adequate prediction was proposed in this work. The approach was based on the use of statistical results as logical functions, which were: range of prediction, critical value of $D_{\mathrm{mod}}X$ (D_{crit}), and confidence limit of Hotelling T^2.

The approach called first for the in-line computation, as part of the sensing strategy, of the logical functions in parallel with the concentration prediction by the multiple linear multivariate PLS calibration model set selected and then, for the selection of the correct prediction following several steps as described later. The approach was validated predicting the concentration of several mixtures with different

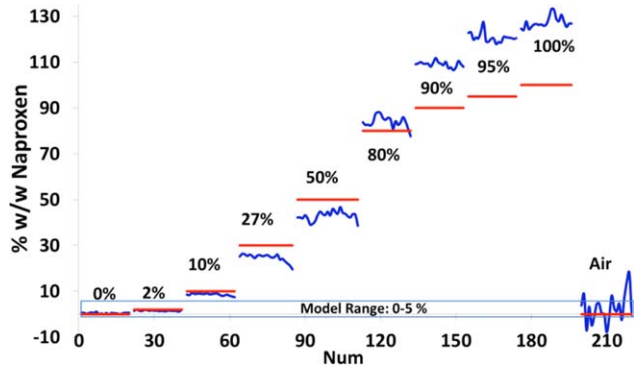

Figure 7. Prediction of all validation blends by the model 0–5% of the MCS-9.

[Color figure can be viewed in the online issue, which is available at wileyonlinelibrary.com.]

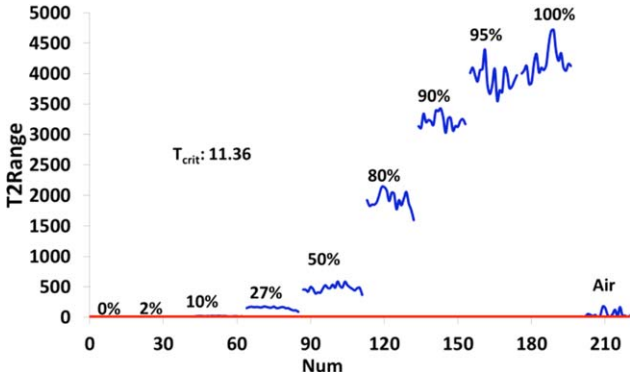

Figure 9. Hotelling T^2 results corresponding to the predictions in Figure 77.

[Color figure can be viewed in the online issue, which is available at wileyonlinelibrary.com.]

concentrations: 0, 2, 10, 27, 50, 80, 90, 95, and 100% API (w/w). This was done to simulate normal events that could happen in the real process. For the sake of space, only the prediction of these blends by the 0–5% model from the MCS-9 is presented in Figure 7.

After all the models had computed their corresponding values, the first logical function in the algorithm consisted in accepting only the predicted values calculated within the range of concentration of the model making the prediction. Any predicted value out of the concentration range for which the model was developed is not reliable. As can be seen in Figure 7, the validation samples 0 and 2% were predicted with a very small error, whereas the predictions for the validation samples 10, 27, 50, 80, 90, 95, and 100, were way off the actual value. In addition, if the behavior of the curve be linear, the 0–5% model would have predicted all the concentrations with similar error to that obtained for 0 and 2%. This confirms once more that the entire curve is not linear. Similar results were obtained with other models, such as 25–30% model and 75–100% model. It is possible that more than one model could make a prediction within their own range, which makes the use of the parameters $D_{mod}X$ and Hotelling T^2 even more critical when selecting the correct prediction.

Once the model is selected, the second logical function was $D_{mod}X$. Figure 8 depicts how the $D_{mod}X$ can be used to discriminate the model that must be used to predict the concentration. Figure 8 depicts that the prediction of the validation mixtures of 27, 50, 80, 90, 95, and 100% had $D_{mod}X$ values greater than the critical value of the 0–5% model, and that only the 0 and 2% samples complied with the D_{crit}. The value of $D_{mod}X$ above the critical value indicates that the spectral data of the validation mixtures not in compliance were significantly different of those used to build the 0–5% model and, therefore, can be rejected. Identical behavior was obtained for the two other models and all the validation blends.

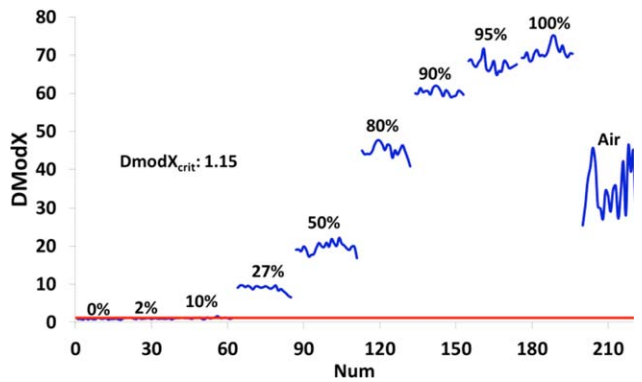

Figure 8. Plot of $D_{mod}X$ values for the prediction in Figure 77.

[Color figure can be viewed in the online issue, which is available at wileyonlinelibrary.com.]

The third and last logical function used to confirm the good prediction was the Hotelling T^2. Figure 9 depicts that the 0–5% model produced Hotelling T^2 values for 0 and 2% concentrations lower than the confidence limit of 99%, whereas the rest of the concentrations had values larger than the 99% confidence limit. Any Hotelling T^2 value larger than the critical limit of 99% indicates that the spectra data of the validation sample were far from the spectral data used to build the model in the score space and, therefore, the predicted value must not be accepted. Again, the other two models exhibited the same performance.

Figure 10 depicts the flowchart to implement the novel approach. It begins with the collection of the NIR spectrum of the sample of interest and continues with the prediction from all models (represented by segment $-1, \ldots$) in parallel. Again, the number of linear multivariate PLS calibration models must be determined off-line as explained in Section Development of the multiple linear multivariate calibration models using PLS. After the prediction, each value is subjected to the three criteria and the one complying with the three criteria is selected as the correct one. In the case that two models meet the criteria, for an actual value close to the common border, the algorithm can be augmented to pick up the prediction from the model with the smallest $D_{mod}X$ out of the two, as this insures the spectrum from the actual value matches better the spectra of this model.

Table 3 presents the results obtained for a sample with 27% API as the actual value from the algorithm in Figure 10 using all the models of the set MCS-9. Applying the first logics, range of prediction, the prediction of the model 25–30% is selected. The second logics, critical value of $D_{mod}X$, picked the same prediction, similarly to the third logics, T^2 value. The rest of the predictions did not pass the filter of the three criteria.

As demonstrated here, the employment of the three criteria insures the selection of a predicted value that will have a very small error. The use of these three logical functions goes

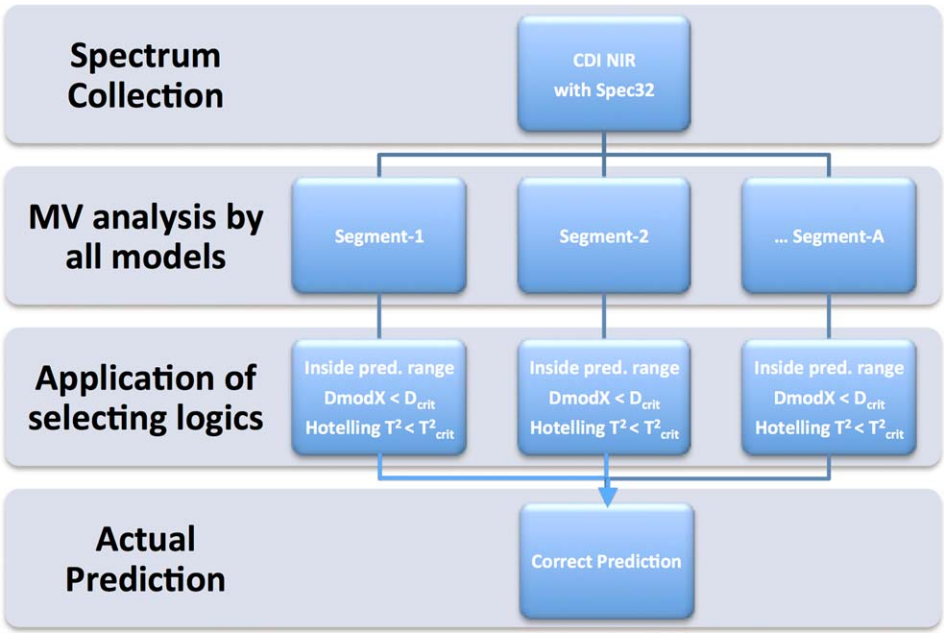

Figure 10. Flowchart of algorithm to select the correct prediction.

[Color figure can be viewed in the online issue, which is available at wileyonlinelibrary.com.]

Table 3. Predictions and Statistics of MCS-9 for a 27% API Sample

	0–5	5–10	10–15	15–20	20–25	25–30	30–50	50–75	75–100
Pred. (avg.)	24.8	23.5	24.8	25.5	26.6	26.8	27.4	36.3	59.4
$D_{mod}X$	8.9	5.8	3.6	1.6	1.1	0.9	1.01	1.3	4.0
Hotelling T^2	155.2	71.8	46.4	22.4	15.2	4.5	5.3	45.4	11.4
RMSEP	2.29	3.3	2.0	1.5	0.7	0.52	0.8	8.5	29.7
Error (%)	8.5	12.3	7.5	5.51	2.5	1.9	3.0	31.67	110.2

further: it permitted the identification of abnormal situation in the process, such as in the case when the powder was not flowing out of the continuous mixer and the NIR sensor was taking spectral data of air. Figures 7 and 9 show that the prediction of the air spectral data was accepted based on the first and third logical functions, where the prediction are between the prediction range and in the confidence limit of Hotelling T^2. Figure 8 shows that the prediction of the air spectral data should be rejected as per the $D_{mod}X$ values, which were greater that the D_{crit}. This means that this spectral data were different than the work set used to build the multiple linear multivariate PLS calibration models.

Figure 11 summarizes how the RMSEP and the average RSD decreased, up to achieving the least minimum possible value, as the number of segments in the set increased. As can be seen from this figure, a blend could pass or fail the FDA acceptance criterion (www.fda.gov/iceci/inspectionguides/ucm074928) depending on the number of models used. The results in Figure 11 were obtained considering the predictions by each of the sets of all the validation blends: 0, 2, 10, 27, 50, 80, 90, 95, and 100% API. One model for the entire range had the worst results [RMSEP (8.7) and RSD (6.5%)] and MCS-6 and above produced adequate predictions, comparable to those obtained by the Spline-PLS, Poly-PLS, and ANN in Ref. 30. The flowchart in Figure 10 with the three criteria (range of prediction, $D_{mod}X$, and Hotelling T^2) was used to select the correct predictions, which were then used to compute both parameters.

Conclusions

The capability of NIR spectroscopy to predict powder concentration with high accuracy had previously been demonstrated, though the range of the linear multivariate calibration models has been rather narrow. This work presented an

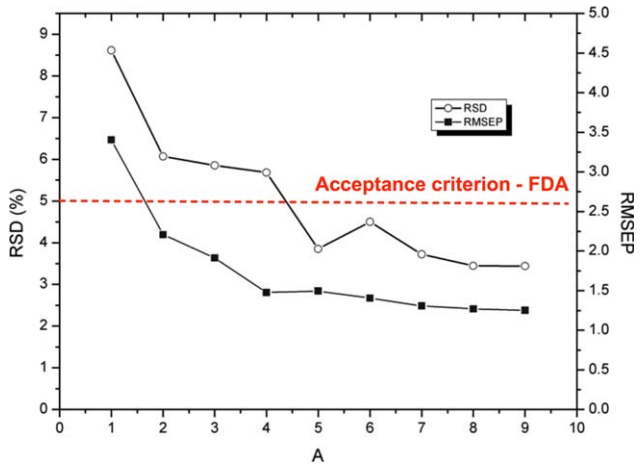

Figure 11. Root Mean Standard Prediction Error and RSD Plot as a function of the number of linear multivariate NIR calibration models set (MCS-A).

[Color figure can be viewed in the online issue, which is available at wileyonlinelibrary.com.]

approach based on the use of multiple NIR linear multivariate PLS calibration models, with just one degree of freedom, to predict in-line a larger concentration range, which exhibited a nonlinear behavior of the NIR absorbance as a function of the solute concentration. The approach was validated predicting the concentration from 0 to 100% in a continuous mixing process. The use of the multiple linear multivariate PLS calibration models increased the accuracy of the NIR sensor to similar to those obtained from nonlinear techniques (Spline-PLS, Poly-PLS, and ANN),[30] as each linear multivariate PLS calibration model covered narrower ranges of concentration, reducing the effect of nonlinearity of the absorbance curve.

It was found in this study that a calibration set of six or more linear multivariate calibration models was sufficient to perform highly accurate predictions of the API concentration in the entire range. The use of the $D_{\text{mod}}X$ and Hotelling T^2 statistics was appropriate functions to select the correct in-line prediction with the multiple calibration set. An algorithm can be implemented to continuously execute these statistics in parallel with the prediction to select the predicted value that complies with all the criteria.

The use of this approach enables the implementation of a better control of the continuous mixing. It has been established in the literature that "bad" measurements affect the performance of any control algorithm. By increasing the accuracy of the prediction at any situation, this strategy helps the control algorithm to decide the actions in the process based on the real disturbance rather than on a bad prediction. This benefit will be demonstrated in a separate work. In addition, the use of multiple linear multivariate PLS calibration model sets could be implemented for other components in the blend or in other processes, in which there are problems with accuracy in the prediction of a variable that exhibits nonlinear behavior.

Acknowledgment

The authors are grateful for the software donation (SIMCA P+) by Umetrics and the financial support from the NSF sponsored project ERC for Structured Organic Particulate Systems (EEC-0540855).

Literature Cited

1. Corredor CC, Bu D, Both D. Comparison of near infrared and microwave resonance sensors for at-line moisture determination in powders and tablets. *Anal Chim Acta*. 2011;696(1–2):84–93.
2. Kogermann K, Zeitler JA, Rantanen J, Rades T, Taday PF, M Pepper, Heinämäki J, Strachan CJ. Investigating dehydration from compacts using terahertz pulsed, Raman, and near-infrared spectroscopy. *Appl Spectrosc*. 2007;61(12):1265–1274.
3. Leskinen JTT, Okkonen M-AH, Toiviainen MM, Poutiainen S, Tenhunen M, Teppola P, Lappalainen R, Ketolainen J, Järvinen K. Lab-scale fluidized bed granulator instrumented with non-invasive process monitoring devices. *Chem Eng J*. 2010;164(2–3):268–274.
4. Rantanen J, Lehtola S, Rämet P, Mannermaa J-P, Yliruusi J. On-line monitoring of moisture content in an instrumented fluidized bed granulator with a multi-channel NIR moisture sensor. *Powder Technol*. 1998;99(2):163–170.
5. Aruna S, Bhagavannarayana G, Sagayaraj P. Investigation on the physicochemical properties of nonlinear optical (NLO) single crystal: l-histidinium dinitrate. *J Cryst Growth*. 2007;304(1):184–190.
6. Bellamy LJ, Nordon A, Littlejohn D. Effects of particle size and cohesive properties on mixing studied by non-contact NIR. *Int J Pharm*. 2008;361(1–2):87–91.
7. Blanco M, Cueva-Mestanza R, Peguero A. Controlling individual steps in the production process of paracetamol tablets by use of NIR spectroscopy. *J Pharm Biomed Anal*. 2010;51(4):797–804.
8. Zhao F, Chen X, Xu N, Lub P, Zheng J-G, Su Q, Wu M. Controlled growth of Cu2S hexagonal microdisks and their optical properties. *J Phys Chem Solids*. 2006;67(8):1786–1791.
9. Allan P, Bellamy LJ, Nordon A, Littlejohn D. Non-invasive monitoring of the mixing of pharmaceutical powders by broadband acoustic emission. *Analyst*. 2010;135(3):518–524.
10. Vanarase AU, Alcalà M, Jerez-Rozo JI, Muzzio FJ, Romañach RJ. Real-time monitoring of drug concentration in a continuous powder mixing process using NIR spectroscopy. *Chem Eng Sci*. 2010;65(21):5728–5733.
11. Puchert T, Holzhauer C-V, Menezes JC, Lochmann D, Reich G. A new PAT/QbD approach for the determination of blend homogeneity: combination of on-line NIRS analysis with PC scores distance analysis (PC-SDA). *Eur J Pharm Biopharm*. 2011;78(1):173–182.
12. De Beer T, Burggraeve A, Fonteyne M, Saerens L, Remon JP, Vervaet C. Near infrared and Raman spectroscopy for the in-process monitoring of pharmaceutical production processes. *Int J Pharm*. 2011;417(1–2):32–47.
13. Storme-Paris I, Clarot I, Esposito S, Chaumeil JC, Nicolas A, Brion F, Rieutord A, Chaminade P. Near infrared spectroscopy homogeneity evaluation of complex powder blends in a small-scale pharmaceutical preformulation process, a real-life application. *Eur J Pharm Biopharm*. 2009;72(1):189–198.
14. Arratia PE, Duong N, Muzzio FJ, Godbole P, Reynolds S. A study of the mixing and segregation mechanisms in the Bohle Tote blender via DEM simulations. *Powder Technol*. 2006;164(1):50–57.
15. Portillo PM, Ierapetritou MG, Muzzio FJ. Characterization of continuous convective powder mixing processes. *Powder Technol*. 2008;182(3):368–378.
16. Koller DM, Posch A, Hörl G, Voura C, Radl S, Urbanetz N, Fraser SD, Tritthart W, Reiter F, Schlingmann M, Khinast JG. Continuous quantitative monitoring of powder mixing dynamics by near-infrared spectroscopy. *Powder Technol*. 2011;205(1–3):87–96.
17. Ely D, Chamarthy S, Carvajal MT. An investigation into low dose blend uniformity and segregation determination using NIR spectroscopy. *Colloids Surf A Physicochem Eng Asp*. 2006;288(1–3):71–76.
18. Arratia PE, Duong N, Muzzio FJ, Godbole P, Lange A, Reynolds S. Characterizing mixing and lubrication in the Bohle Bin blender. *Powder Technol*. 2006;161(3):202–208.
19. Ramachandran R, Ansari MA, Chaudhury A, Kapadia A, Prakash AV, Stepanek F. A quantitative assessment of the influence of primary particle size polydispersity on granule inhomogeneity. *Chem Eng Sci*. 2012;71:104–110.
20. Berntsson O, Danielsson L-G, Lagerholm B, Folestad S. Quantitative in-line monitoring of powder blending by near infrared reflection spectroscopy. *Powder Technol*. 2002;123(2–3):185–193.
21. Palou A, Cruz J, Blanco M, Tomàs J, de los Ríos J, Alcalà M. Determination of drug, excipients and coating distribution in pharmaceutical tablets using NIR-CI. *J Pharm Anal*. 2012;2(2):90–97.
22. Beuermann S, Buback M, Gadermann M, Jürgens M, Saggu DP. Tubular reactor synthesis of styrene–methacrylate copolymers in solution with supercritical carbon dioxide. *J Supercrit Fluids*. 2006;39(2):246–252.
23. Dias AM, Moita I, Alves MM, Ferreira EC, Páscoa R, Lopes JA. Activated sludge process monitoring through in situ near-infrared spectral analysis. *Water Sci Technol*. 2008;57(10):1643–1650.
24. Hongqiang L, Hongzhang C. Near-infrared spectroscopy with a fiber-optic probe for state variables determination in solid-state fermentation. *Process Biochem*. 2008;43(5):511–516.
25. Balabin RM, Syunyaev RZ. Petroleum resins adsorption onto quartz sand: near infrared (NIR) spectroscopy study. *J Colloid Interface Sci*. 2008;318(2):167–174.
26. Balabin RM, Syunyaev RZ, Schmid T, Stadler J, Lomakina EI, Zenobi R. Asphaltene adsorption onto an iron surface: combined near-infrared (NIR), Raman, and AFM study of the kinetics, thermodynamics, and layer structure. *Energy Fuels*. 2011;25(1):189–196.
27. Syunyaev RZ, Balabin RM, Akhatov IS, Safieva JO. Adsorption of petroleum asphaltenes onto reservoir rock sands studied by near-infrared (NIR) spectroscopy. *Energy Fuels*. 2009;23(3):1230–1236.
28. Portillo PM, Ierapetritou MG, Muzzio FJ. Effects of rotation rate, mixing angle, and cohesion in two continuous powder mixers—a statistical approach. *Powder Technol*. 2009;194(3):217–227.
29. Shao L, Liu B, Griffiths PR, Leytem AB. Using multiple calibration sets to improve the quantitative accuracy of partial least squares (PLS) regression on open-path Fourier transform infrared

(OP/FT-IR) spectra of ammonia over wide concentration ranges. *Appl Spectrosc*. 2011;65(7):820–824.
30. Balabin RM, Safieva RZ, Lomakina EI. Comparison of linear and nonlinear calibration models based on near infrared (NIR) spectroscopy data for gasoline properties prediction. *Chemometr Intell Lab Syst*. 2007;88:183–188.
31. Eriksson L, Johansson E, Kettaneh-Wold N, Trygg J, Wikström C, Wold S. *Multi- and Megavariate Data Analysis. Basic Principles and Applications, 2nd ed*. Umeå (SE): Umetrics AB, 2006.

Appendix

Distance to Model in X-space ($D_{\text{mod}}\ X$) is a statistical parameter used to measure how different is a spectral from a work set used to build a calibration model. $D_{\text{mod}}X$ is computed for each spectral following the equation

$$S_i = \sqrt{\frac{\sum_{k=1}^{K} e_{ik}}{(K-A)}}$$

S_i is the absolute distance to the model of a spectral in the calibration model, K is the number of variables, A is the number of PCs, e_{ik} is the residual of the spectral

$$S_o = \sqrt{\frac{\sum_{i,j} e_{ij}}{(K-A)(N-A-1)}}$$

S_o is the average residual of the calibration model, where N is the number of samples and e_{ij} is the residual of the calibration model.

The normalized distance to the model is obtained dividing S_i by S_o. $(S_i/S_o)^2$ has an approximated F distribution with degrees of freedom of the calibration model and spectral. This is used to compute the critical distance to the model D_{crit} for new observations, at the desired probability level. Spectral data with a normalized distance to model is considered as outliers if the distance is larger than the critical distance.[31]

Manuscript received Sep. 13, 2013, and revision received May 7, 2014.